Effects of Substrate Residue on the Frequency Response of High-Tone Bulk Acoustic Resonator

Re-Ching Lin, Ying-Chung Chen, Po-Tsung Hsieh
Department of Electrical Engineering
National Sun Yat-Sen University
Kaohsiung, Taiwan
p923010003@student.nsysu.edu.tw

Kuo-Sheng Kao
Department of Computer and Communication
SHU-TE University
Kaohsiung, Taiwan
kks@mail.stu.edu.tw

Chih-Ming Wang
Department of Electrical Engineering
Cheng Shiu University
Kaohsiung, Taiwan
cmwang.email@msa.hinet.net

***Abstract*—The high-tone bulk acoustic resonator (HBAR), consisted of a Mo/ZnO/Pt/Ti/Si structure, is fabricated. The thickness of Si substrate under HBAR is controlled by a two-step process of wet- and dry-etching. The resonance frequency spacing (Δf) of HBAR is dependent on the etching duration. The frequency response of the HBAR is measured using an HP8720 network analyzer and a CASCADE probe station. The estimation of Si residue based on the high-tone resonant phenomenon coincides with practical measurements. A frequency response with no harmonic resonance, which is an extreme case of HBAR without Si residue, is revealed. Furthermore, a sensor of high-frequency bulk acoustic wave resonator is obtained.**

I. INTRODUCTION

Recently, the film bulk acoustic resonator (FBAR) filter has been widely adopted in modern communication systems. The performance of an FBAR device is better than other dielectric ceramic and surface acoustic wave (SAW) filters due to its inherent advantages such as low insertion loss, high power handling capability and small size. On the other hand, when the substrate residue is significantly thicker than that of the piezoelectric film, the phenomenon of high-tone resonances arises and the high-tone bulk acoustic resonator (HBAR) forms [1, 2].

The HBAR has multiple resonant responses with equal resonance frequency spacing (Δf), which is determined by the ratio of film thickness to substrate residue. Besides, the loading effect on the surface of the resonant region will cause the resonant frequency shift. Based on the measurement of frequency responses, the substrate residue or mass adhesion can be estimated precisely [3-5].

For sensor applications, a high-Q resonator that provides a precise frequency is essential. Once the operating frequency of a mass sensor increases to GHz range, the frequency variation caused by the micro mass can be detected easily. When the resonant frequency of an HBAR exceeds GHz, which is hundreds of times higher than that of the quartz crystal microbalance (QCM), HBAR device will be a suitable candidate for nanotechnology applications [6]. Besides, the HBAR sensor has a sturdy structure and can be easily integrated into the integrated circuits (IC).

In general, the schematic diagram of an HBAR, consisting of the composite structures of top electrode, piezoelectric layer, bottom electrode and membrane, can be presented as Fig. 1. Based on the Mason equivalent circuit, the equivalent impedance between the top and bottom electrodes is

$$Z_{in} = \frac{1}{j\omega C_0}\left[1 - \frac{k_t^2}{\gamma_p}\frac{(z_1+z_2)\sin\gamma_p + j2(1-\cos\gamma_p)}{(z_1+z_2)\cos\gamma_p + j(1+z_1z_2)\sin\gamma_p}\right] \quad (1)$$

where $z_1=Z_1/Z_o$ and $z_2=Z_2/Z_o$ are equivalent impedances on the top and bottom surfaces of the piezoelectric layer normalized to the acoustic impedance of piezoelectric layer Z_o, respectively; C_0 is static capacitance between the top and bottom electrodes; γ_p is equal to $2\pi f l_p/v_p$ and is the phase delay of the piezoelectric layer; l_p and v_p are the thickness and acoustic wave velocity of piezoelectric layer, respectively; k_t^2 is the electromechanical coupling coefficient of the piezoelectric layer [7-9]. Based on the data of materials, the resonant frequency of various modes can be evaluated and the frequency spectra of HBAR can be observed in a specific frequency range. In this study, the varied frequency responses of HBAR devices caused by substrate residue or additional deposited materials will be investigated.

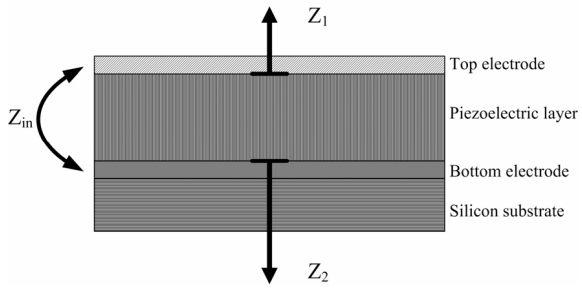

Figure 1. The schematic diagram of an HBAR resonator.

II. EXPERIMENT

TABLE I. DEPOSITION PARAMETERS OF ZNO THIN FILMS

Substrate	Pt/Ti/SiN_x/Si
Substrate temperature	R.T.
Substrate to target distance	50 mm
Target	Zn (2 inch dia..)
Residual pressure	2×10^{-6} Torr
rf power	80W
Sputtering pressure	15 mTorr
Ar gas flow rate	1st step: 1.9 sccm 2nd step: 3.7 sccm
O_2 gas flow rate	1st step: 5.6 sccm 2nd step: 3.8 sccm

Silicon (100) wafers coated with low-stress silicon nitride layers, grown by low-pressure chemical vapor deposition (LPCVD), were employed as substrates. The low-stress silicon nitride layers were utilized as supporting membranes in integrated FBAR (or HBAR) devices. Figure 2 presents the fabrication processes for the device. The bottom electrode of Pt was deposited onto the Ti seeding layer without heating the substrate by DC magnetron sputtering.

The piezoelectric thin film was deposited by reactive radio frequency (rf) magnetron sputtering in a two-step process. The base pressure of the sputtering system was evacuated to 2×10^{-6} Torr using a diffusion pump. The working pressure and rf power were 15 mTorr and 80 W, respectively. The ratios of gas flow rate (O_2 /Ar+O_2) for the first and second steps were 75% and 50%, respectively. Table I presents the detailed deposition parameters of the ZnO piezoelectric layer.

Stress is inherent in the multi-layer structure. Although the piezoelectric layer is deposited with a heated substrate holder; stress is hard to avoid [10]. Excess stress at the cavity edge will lead to failure of the etching stop layer of low-stress silicon nitride. In this study, we adopted a two-step etching process, which combined the wet etching process with high etching rate and the dry etching process with moderate etching rate. The wet etching process adopts KOH as the etching solution, and the reaction ion etching (RIE) is carried out for the second step to remove the residual substrate and reduce destructiveness caused by using only KOH process.

The HBAR is formed as the structure of Mo/ZnO/Pt/Ti/Si. The frequency spacing (Δf) of HBAR is defined as

$$\Delta f = \frac{v_p}{(l_{sb} + l_p)} \qquad (2)$$

where v_p is the acoustic velocity of the ZnO. The l_p and l_{sb} are thicknesses of the ZnO and Si residues, respectively. [6] As derived from Eq. (2), Δf is quite small prior to substrate etching, and increases with the decreased Si residues. Therefore, the frequency spectrums of the devices with various etching times are obtained. Notably, RIE dry etching is carried out for the final stage of manufacturing. Table II presents the RIE parameters.

The preferred orientation and crystal properties of the ZnO film were evaluated by X-ray diffraction (XRD) using a SHIMADZU XRD-6000 with CuK_α radiation. The cross sections of grain structure of the ZnO films were observed by scanning electric microscopy (SEM) (Philips XL40 FESEM). The HP8720 network analyzer and CASCADE probe station (RHM-06/V + GSG 150) were utilized to measure the frequency responses of the HBAR devices.

TABLE II. PARAMETERS OF RIE DRY ETCHING PROCESS.

RF power (W)	**Work pressure (mTorr)**	**Temperature (℃)**	**DC bias (V)**	**Gas flow**	
				SF_6 (sccm)	***O_2 (sccm)***
50	100	R. T.	30	50	10

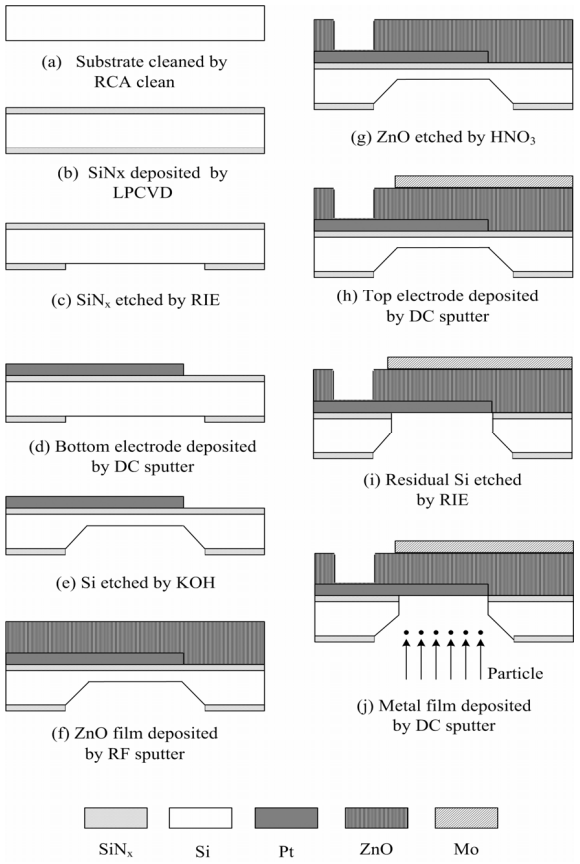

Figure 2.The fabrication processes of an HBAR device.

III. RESULTS AND DISCUSSION

The bottom electrode with low surface roughness, high conductivity, and good adhesion to substrate was obtained in this study. The ZnO film with (002) preferred orientation and smooth surface were also obtained using the two-step deposition process. Figure 3 shows the XRD pattern and cross-sectional image of ZnO/Pt/Ti/SiN_x/Si structure, which reveals the strong ZnO(002) preferred orientation and texture.

Generally, Si etched by wet etching using 30 wt% KOH solution at 100 ℃ is quick and cost effective; however, wet etching is very destructive. The dry etching using RIE is expected to be moderate and obviously time consuming. The etching rates for wet and dry etching are 253 μm/h and 90 μm/h, respectively (Fig. 4). The distinguishable features of the two methods are contradictory, and hence, two-step etching process for cavity fabrication is optimal.

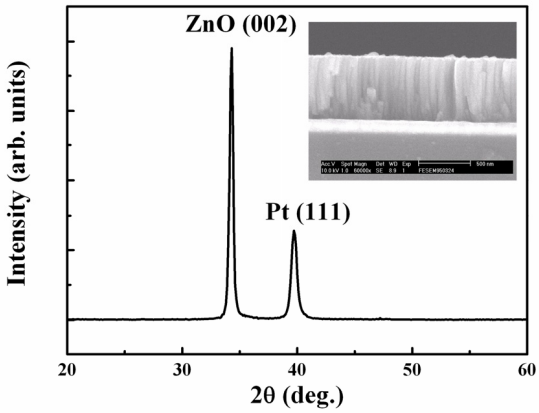

Figure 3. XRD pattern and SEM cross-section of ZnO films deposited on Pt/Ti/SiN_x/Si.

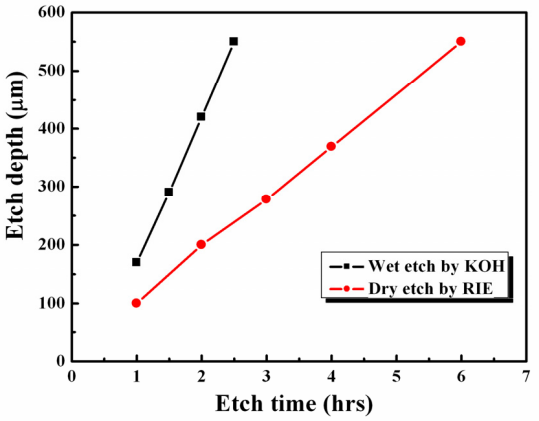

Figure 4. Etching rate of Si by KOH wet-etching and RIE dry-etching .

The Si residue can be calculated using Eq. (2). Figure 5 shows cavities images with and without Si residue. The bottom electrode is obvious after dry etching. The Si residue can be controlled accurately by dry etching duration.

Figure 6 presents the frequency responses with and without Si residue. The center frequency and coupling coefficients are 2208.4375 MHz and 6.7%, respectively, for the FBAR without Si residue.

The impedances of Z_1 and Z_2 can be described as

$$Z_1 = jZ_{e1}\tan\gamma_{e1} \tag{3}$$

$$Z_2 = j\frac{Z_{sb}\tan\gamma_{sb} + Z_{e2}\tan\gamma_{e2}}{1-\left(Z_{sb}/Z_{e2}\right)\tan\gamma_{e2}\tan\gamma_{sb}} \tag{4}$$

where Z_{e1}, Z_{e2} and Z_{sb} are acoustic impedances of the top electrode, bottom electrode and substrate, respectively, and γ_{e1}, γ_{e2} and γ_{sb} are phase delays of the top electrode, bottom electrode and substrate, respectively.

The variations of silicon substrate residue will change the phase delay of the substrate. As derived from Eq. 4, the $\gamma_{sb}=2\pi f l_{sb}/v_{sb}$ varies with the substrate residue, l_{sb}. Reduction of the substrate residue will reduce the number of variations of phases in the resonate zone. Therefore, Δf will increase as the silicon substrate residue decreases. The single resonant mode of HBAR and FBAR is obtained as no silicon substrate residues exists (Fig. 6).

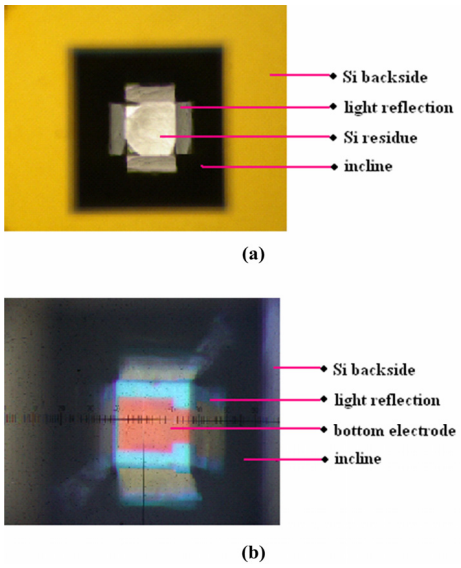

Figure 5. Cavity images of FBAR, (a) with and (b) without Si residue.

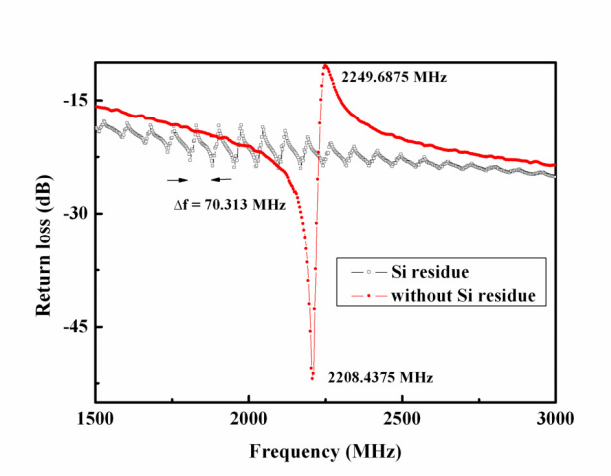

Figure 6. Frequency spectrum of FBAR, (a) with and (b) without Si residue.

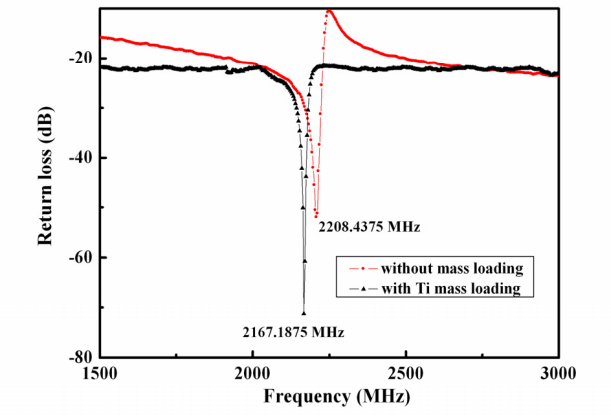

Figure 7. Frequency spectrum of FBAR, (a) with and (b) without mass loading.

The resonant frequency is reduced when excess mass is added to the resonant zone of the FBAR. The vector network analyzer (VNA) places strict limitations on frequency range measurements. The default aperture is the total frequency span divided by the number of points. Therefore, the VNA provides the best resolution for a given bandwidth with the highest number of points selected. The resonant frequency is decreased from 2208.4375 MHz to 2167.1875 MHz due to the Ti deposited on the resonant zone (Fig. 7).

IV. Conclusion

The problem of fracture in fabricating an HBAR device is solved using a two-step etching process, by which, a near 100% yield can be obtained. The residue inside the cavity is removed by dry etching, and the singular resonant frequency response of FBAR is performed. The shift of resonant frequency of 41.25 MHz is associated with 240 nm deposition of Ti. Therefore, the phenomenon of resonant frequency variation can be applied as a mass sensor.

Acknowledgment

The authors would like to thank the National Science Council of the Republic of China, Taiwan, for financially supporting this research under Contract Nos. NSC95-2221-E-110 -029 and NSC95-2221-E-366-022.

References

[1] K. M Lakin, J. Belsick, J. F. McDonald, and K. T. McCarron, "Improved Bulk Wave Coupling Coefficient for Wide Bandwidth Filters," in *Proc. IEEE Ultrason. Symp.*, 2001, pp. 827-831.

[2] K. W. Kim, G. Y. Kim, J. G. Yook, and H. K. Park, "Air-Gap-Type TFBAR-Based Filter Topologies," *Microwave and Optical Technology Lett.*, vol. 34, pp. 386-387, 2002.

[3] K. Nakamura, H. Sasaki, and H. Shimizu, "A Piezoelectric Composite Resonator Consisting of a ZnO Films on an Anisotropically Etched Silicon Substrate," *Jpn. J. Appl. Phys.*, vol. 20, pp. 111-114, 1981.

[4] K. M. Lakin and J. S. Wang, "Acoustic Bulk Wave Composite Resonators," *Appl. Phys. Lett.*, vol 38, pp. 125-127, 1981.

[5] T. W. Grudkowski, J. F. Black, T. M. Reeder, D. E. Culen, and R. A. Wagner, "Fundamental-Mode UHF/VHF Miniature Acoustic Resonator and Filters on Silicon," *Appl. Phys. Let.*, vol. 37, pp. 993-995, 1980.

[6] H. Zhang, W. Pang, and E. S. Kim, "High-frequency Bulk Acoustic Resonant Microbalances in Liquid," in *Proc. IEEE Freq. Contr. Symp.*, 2005, pp. 73-77.

[7] H. Zhang and E. S. Kim, "Micromachined Acoustic Resonant Mass Sensor," *J. Microelectromechanical system*, vol. 14, no. 4, pp. 699-706, 2005.

[8] W. Pang, H. Zhang, J. J. Kim, H. Yu, and E. S. Kim, "High Q Single-Mode High-Tone Bulk Acoustic Resonator Integrated with Surface-Micromachined FBAR Filter," in *Proc. IEEE Microwave Symp.*, 2005, pp. 413-416.

[9] S. Alzuaga, J. M. Friedt, S. Ballandras, J. Masson, L. Robert, N. Bazin, B. Guichardaz, and D. Gachon, "Simulation and Experimental Measurements of High-Overtoned Bulk Acoustic Resonators (H-BAR)," in *Proc. IEEE Ultrason. Symp.*, 2005, pp. 1183-1186.

[10] I. Chung, I. K. Yoo, W. Lee, C. W. Chung, J. K. Lee, and S. B. Desu, "Electrode stress effects on electrical properties of PZT thin film capacitors," in *Proc. IEEE Symp. Appl. Ferro.*, 1995, pp. 527-530.